Fuel 357 (2024) 129589

Contents lists available at ScienceDirect

Fuel

journal homepage: www.elsevier.com/locate/fuel

Full length article

Model optimization of a high-power commercial PEMFC system via an improved grey wolf optimization method

Hongxu Zhou [a,b], Xiaohua Wu [a,b], Yang Li [c], Zhanfeng Fan [d,a,*], Weishan Chen [e], Jianwei Mao [a,b], Pengyi Deng [a,b], Torsten Wik [c]

[a] Vehicle Measurement Control and Safety Key Laboratory of Sichuan Province, Xihua University, Chengdu, 610039, China
[b] Sichuan Engineering Research Center of Intelligent Control and Simulation Test Technology for New Energy Vehicles, Xihua University, Chengdu, 610039, China
[c] Department of Electrical Engineering, Chalmers University of Technology, Gothenburg, 41296, Sweden
[d] School of Architecture and Civil Engineering, Chengdu University, Chengdu, 610106, China
[e] Shanghai Refire Energy and Technology Co., Ltd, Shanghai, 201800, China

ARTICLE INFO

Keywords:
Proton exchange membrane fuel cell
Grey wolf algorithm
Chaotic mapping
Random walk strategy

ABSTRACT

Proton exchange membrane fuel cell (PEMFC) models are conventionally established with a set of parameters identified under steady-state operating conditions. However, such an approach is insufficient to accurately capture the dynamic characteristics of multi-parameter changes in real-world scenarios. This paper develops a semi-empirical model for a 110-kW commercial PEMFC system based on its dynamic operation data to remedy the defects. To improve the fitting accuracy of the semi-empirical PEMFC model, an improved grey wolf optimization (IGWO) algorithm is proposed for model parameter identification. The IGWO algorithm adopts chaotic mapping to optimize the initial population distribution, and a random walk strategy is incorporated to boost the local search ability of the traditional grey wolf optimization (GWO) algorithm. The effectiveness of this IGWO algorithm in optimizing the semi-empirical model is experimentally verified on the 110-kW PEMFC system under highly dynamic operating conditions. Results show that the proposed IGWO algorithm can effectively identify the semi-empirical model's parameters, establishing a stable and robust model that outperforms those based on traditional metaheuristic algorithms such as GWO, particle swarm optimization, and genetic algorithm. The demonstrated improvement renders it as better suited for optimizing PEMFC semi-empirical models under real-world operating conditions.

1. Introduction

1.1. Background

Proton exchange membrane fuel cells (PEMFCs) are widely used in various applications such as mobile power supply, stationary power generation, and electrified transportation systems. They are favored for their high energy density, noise-free operation, utilization of hydrogen as fuel, and minimal emissions, limited to water alone [1,2]. However, the current PEMFC system still faces many technical limitations in its power capability, durability, and reliability, making it difficult to meet the demand for high-power applications [3]. Additionally, the relatively high costs associated with both the PEMFC system and the hydrogen further increase the research expenses of PEMFC technology. Consequently, the importance of modeling and simulation techniques, without relying solely on physical experiments, has been recognized to study the dynamic performance of PEMFC. Accurate models can effectively simulate electrochemical reaction phenomena and facilitate the integrated design of auxiliary systems, providing more insight into fuel cells' operational status. These models enable researchers to predict and comprehend the fuel cells' performance and response characteristics, playing a crucial role in optimizing system design, evaluating performance, and developing control strategies [4,5].

1.2. Literature review

The accurate PEMFC model is built on experimental data, which can be classified into data-driven models [6,7], empirical formula-based models [8–10], and hybrid models [11]. The data-driven models mainly use various neural network (NN) algorithms to describe the input–output relationship. For example, an artificial neural network (ANN) algorithm was used to establish a data-driven model to predict the output performance of a high-temperature PEMFC system [12], where

* Corresponding author at: Vehicle Measurement Control and Safety Key Laboratory of Sichuan Province, Xihua University, Chengdu, 610039, China.
E-mail address: fzhf213@163.com (Z. Fan).

https://doi.org/10.1016/j.fuel.2023.129589
Received 2 July 2023; Received in revised form 12 August 2023; Accepted 20 August 2023
Available online 31 August 2023

the training data were generated from a numerical model. In Ref. [13], a data-driven model was established using radial basis function and applied to a PEMFC system parameters optimization. Two artificial intelligence techniques, including probabilistic NN and group method of data handling (GMDH) method, were investigated in [14] to predict and control the behavior of a 25-W PEMFC. Numerical results showed that the GMDH model was excellent for PEMFC design due to its high accuracy based on polarization experimental data. A teaching–learning optimization and differential evolution-based Elman NN was effectively implemented for PEMFC nonlinear parameter identification [15]. The back propagation NN algorithm was employed to develop the mapping relation model between the membrane reactor's prime operational parameters and fuel cell output performance for a 500-W horizon polymer electrolyte fuel cell system's design and control [16]. Ref. [17] proposed a hybrid model combining a least square vector machine model with a regularized particle filter, which can provide better remaining useful life prediction accuracy for the PEMFC. A Bayesian-gated recurrent unit (GRU) model that combines the Bayesian theory and GRU was proposed in [18] to predict the phenomenon of fuel cell voltage decay over time so that the uncertainty in model parameters is addressed. Since the PEMFC exhibits strong nonlinear characteristics, the output performance is significantly influenced by temperature, reaction gas pressure, and load change rate [19]. Due to the limitation of cost and experimental environment, considering these influencing factors, it is practically challenging to obtain adequate training data from existing voltage and current measurements to reflect the system's characteristics under real-world operating conditions.

Modeling methods based on empirical formulas primarily involve fitting equations to describe the relationship between input and output variables and formulating equations to characterize the electrical properties of circuit components. For instance, Amphlett et al. [20] developed empirical and semi-empirical models for PEMFC. Restrepo et al. [21] improved Amphlett's semi-empirical model by proposing a semi-empirical circuit model, including polarization capacitance phenomena, and validated the model's accuracy using experimental data. Semi-empirical models are widely recognized for their ability to accurately simulate the electrochemical characteristics of PEMFC and predict output performance across various operating conditions, all while minimizing the need for extensive experimental data during model establishment. Based on a semi-empirical PEMFC model and an air supply model, a model reference adaptive control algorithm consisting of a nominal feedback loop and an adaptive mechanism loop was proposed to control the cathode oxygen ratio and improve the performance and efficiency of the air compressor in [22]. Similarly, based on a coupled semi-empirical model and a thermal management model, a temperature fuzzy control strategy, improved by particle swarm optimization (PSO) algorithm, was proposed to optimize the performance of the PEMFC [23]. The effects of altitude variation and air stoichiometry on stack performance and thermal management were investigated by coupling a semi-empirical model with a thermodynamic model in [24]. A differential evolution (DE) algorithm based on a semi-empirical model was designed to optimize a fuzzy logic controller for PEMFC's maximum power point tracking in [25]. An accurate semi-empirical model can better fit the PEMFC output performance. Compared to data-based models, semi-empirical models offer the benefits of a simpler structure and improved model accuracy. In addition, the establishment of semi-empirical models does not rely on a large amount of experimental data. However, it is important to note that for every different PEMFC system the unknown parameters of the semi-empirical model have to be determined under varying operating conditions.

In recent years, growing research has focused on determining, improving, and optimizing the unknown parameters of semi-empirical models for PEMFC systems. Particularly, intelligent optimization technology based on the metaheuristic method has achieved good results in identifying unknown model parameters. The metaheuristic method has been successfully applied to identify PEMFC model parameters, including DE algorithm [26,27], genetic algorithm (GA) [28,29], and PSO algorithm [30–32]. Also, a hybrid adaptive DE algorithm was applied to the PEMFC parameter identification problem, and the superiority of the algorithm was verified through polarization behavior prediction [26]. In [27], a dynamic DE algorithm with a collective guiding factor was proposed to identify the complex parameters of the PEMFC model. It could accurately estimate the PEMFC model parameters from polarization test data. In [28], the effectiveness of the GA in the parameter identification for the semi-empirical models was verified by selecting different ranges of unknown parameters based on polarization data. A novel problem formulation based on the derivative of power to current was proposed and solved via the GA [29]. Its accuracy and convergence characteristics were verified using polarization test data under two different reaction gas pressures and stack temperatures.

However, the traditional GA is known for its complex algorithm structure, slower optimization convergence, and low precision when solving high-dimensional problems. Therefore, a PSO-based parameter identification technique for the Nexa 1.2 kW PEMFC model was proposed in [30]. Furthermore, the momentum PSO was demonstrated to achieve fast convergence for accurate PEMFC modeling [31]. The chaos-embedded PSO algorithm with a new objective function was proposed for PEMFC parameter identification in a more realistic setting in [32]. The optimization effectiveness was validated using polarization test data from three commercial fuel cells, namely 250 W Stack, BCS-500 W stack, and Nedstack PS6.

Unfortunately, the performance of the PSO algorithms depends on the selection of learning and inertia factors. Tuning of these parameters demands high computation costs, and inappropriate settings can lead to premature convergence problems at a later stage. Therefore, in addition to the commonly used GA and PSO, many novel metaheuristic algorithms have been proposed for the parameter identification of the semi-empirical PEMFC model. These include the shark smell optimization (SSO) method [33], golden jackal optimization (GJO) algorithm [34], and grey wolf optimization (GWO) algorithm [35]. For example, the SSO method was used to determine the semi-empirical model's unknown parameters in [33], with validation using the polarization test data of five commercial fuel cell stacks. Similarly, a PSO-based GJO method was developed to reduce the sum of squared errors (SSE) of the measured output voltage and the output voltage of the PEMFC stack in [34]. The results revealed that it outperformed the other methods under comparison in optimally estimating the PEMFC model.

Most literature establishes the PEMFC model based on public polarization experimental data. In these data, the operating parameters, including the reaction gas pressure and temperature, exhibits a relatively stable profile, while load variations occur gradually. However, there are significant differences between the polarization experimental data and real-world conditions. There, the load current undergoes rapid changes, while the operating parameters, such as temperature and reaction gas pressure, display significant variations. In the works mentioned above, Refs. [29,33,35] used polarization experimental data under different gas pressure and temperature to verify the accuracy of the model. The results showed that temperatures and reaction gas pressures greatly impacted on the performance of the PEMFC and the accuracy of the model. Therefore, the parameter identification of primary significance should be based on the actual dynamic conditions.

While various metaheuristic methods have successfully identified and optimized PEMFC model parameters, each method possesses distinct characteristics and is best suited for specific optimization problems, considering factors such as the number of parameters involved, exploration and exploitation strategies, and other relevant considerations. Furthermore, metaheuristic algorithms inherently suffer from certain limitations, including sensitivity to population initialization settings, susceptibility to local optima, and premature convergence. Therefore, there is potential for enhancing the accuracy of these algorithms

to a certain degree [36,37]. Compared to other search optimization algorithms, the GWO algorithm has the advantages of simple structure, easy programming, fewer parameter settings, and fast iteration [38,39]. Therefore, it has been commonly applied in parameter identification and system optimization. In [35], the PEMFC model based on GWO was proposed and compared with other algorithms published in the literature. A hybrid GWO method, including crossover and mutation operators, was proposed for parameter identification of a PEMFC system [40], to enhance the global search capability and effectively avoid local optima.

For GWO, the initial population position, convergence factor, and the update formula of the entire wolf pack position has a specific influence on the optimization performance, leading to the problems of poor population diversity and slow convergence in later iterations [41,42]. The traditional metaheuristic algorithm uses pseudorandom numbers to generate the initial population position, which tends to cause problems of uneven population initialization and slow convergence of the algorithm. A chaotic system has the characteristics of randomness, ergodicity, and regularity, which can effectively overcome the shortcomings of pseudorandom number initialization of the population. For example, in [43], a chaotic random sequence was employed to generate the initial population of GA. This strategy effectively addressed the traditional GA's dependence on the initial value, improving the performance. Similarly, in [44], the chaos operator was used to simultaneously optimize the initial population as well as the random walk strategy of the ant colony algorithm.

In summary, over the past few years, the development of semi-empirical modeling approaches has provided effective means of reducing testing costs and circumventing the requirement for extensive experimental data. The application of various metaheuristic methods to parameter identification of the PEMFC has yielded successful results. However, it is worth noting that each method possesses distinct characteristics concerning the optimization of parameters, exploration, and exploitation strategies. Consequently, these variations can impose limitations on the accuracy of the algorithms.

This paper employs an improved grey wolf optimization (IGWO) algorithm for refining the semi-empirical PEMFC model. It utilizes a chaotic mapping approach to initialize the population distribution of the GWO algorithm. This results in a well-balanced population distribution across the search range, effectively enhancing population diversity. An improved iteration factor employing the cosine function is designed to achieve a harmonious balance between global and local search capabilities during the early and later iterations of the GWO algorithm. Furthermore, during the latter iterations of the IGWO algorithm, the grey wolf elite individual random walk strategy is incorporated to enhance the local search ability of the GWO algorithm.

1.3. Contributions

This paper presents two key contributions to address the challenges of PEMFC dynamic modeling.

First, a semi-empirical model is developed based on experimental data obtained from dynamic conditions of a high-power commercial PEMFC system. The model captures the multi-parameter dynamics and comprehensively represents the system's behavior.

Second, the IGWO algorithm leverages chaotic mapping and a random walk strategy to optimize the model parameters, enhancing its accuracy and suitability for dynamic operating scenarios. The effectiveness of the IGWO algorithm in optimizing the semi-empirical model under dynamic conditions is demonstrated. A comparative analysis with traditional optimization algorithms, including GWO, PSO, and GA, highlights the superior performance of IGWO.

The proposed methodology offers significant advancements in modeling PEMFC systems by incorporating dynamic characteristics and addressing the limitations of traditional optimization techniques. The results highlight the efficacy of the IGWO algorithm in optimizing the semi-empirical model, paving the way for improved system performance and control strategies in dynamic PEMFC applications.

1.4. Outline

The remainder of the paper proceeds as follows. The PEMFC model is introduced in Section 2. Section 3 details the parameter identification method of the semi-empirical PEMFC model. The corresponding experimental results are discussed in Section 4, followed by the conclusions in Section 5.

2. PEMFC model

We adopt the PEMFC model developed in [32–35] to describe the input–output relationship of the PEMFC system under investigation. In practical operations, the cell voltage V_{fc} is significantly lower than the open-circuit voltage (OCV) E_{Ne} due to various voltage losses. This is given by

$$V_{fc} = E_{Ne} - V_{Act} - V_{Con} - V_{Ohm} \tag{1}$$

where V_{Act}, V_{Con}, and V_{Ohm} are voltage losses due to activation, concentration polarization, and ohmic polarization, respectively. The OCV E_{Ne} is the ideal potential of the PEMFC obtained from the Nernst equation, i.e.,

$$E_{Ne} = 1.229 - 0.000845(T_{fc} - 298.15) + 0.0000413T_{fc}\ln(P_{H_2}P_{O_2}^{0.5}) \tag{2}$$

where T_{fc} is the temperature of the PEMFC. P_{H_2} and P_{O_2} represent the gas pressures of the hydrogen and the oxygen in the reaction, respectively.

The activation polarization voltage loss V_{Act} is the result of the driving voltage required by the electrode reaction kinetics. It can be expressed as

$$V_{Act} = -[\zeta_1 + \zeta_2 T_{fc} + \zeta_3 T_{fc}\ln(M_{O_2}) + \zeta_4 T_{fc}\ln(I_{fc})] \tag{3}$$

$$M_{O_2} = \frac{P_{O_2}}{5.08\times10^6}\exp\left(\frac{498}{T_{fc}}\right) \tag{4}$$

where ζ_1, ζ_2, ζ_3, and ζ_4 are four coefficients, I_{fc} denotes the load current, and M_{O_2} represents the oxygen molar concentration.

The concentration polarization V_{Con} is the consequence of the rapid consumption of reactants on the electrode, which forms a concentration gradient. The electrochemical reaction potential will change with the load current, which can be expressed as

$$V_{Con} = -\beta\ln\left(1 - \frac{I_{fc}}{I_{max}}\right) \tag{5}$$

where β is a fitting parameter to be identified and I_{max} is the limiting maximum current.

The ohmic polarization V_{Ohm} includes the intrinsic electronic impedance and the membrane ionic impedance of conducting materials, expressed as

$$V_{Ohm} = I_{fc}(R_m + R_c) \tag{6}$$

where

$$R_m = \frac{\rho_m l}{A_{fc}} \tag{7}$$

$$\rho_m = \frac{181.6[1 + 0.03\frac{I_{fc}}{A_{fc}} + 0.062(\frac{T_{fc}}{303})^2(\frac{I_{fc}}{A_{fc}})^{2.5}]}{[\lambda - 0.634 - 3(\frac{I_{fc}}{A_{fc}})]\exp(4.18\frac{T_{fc}-303}{T_{fc}})} \tag{8}$$

Here, R_m and R_c are the membrane ionic and material electronic resistance, respectively. Furthermore, ρ_m is the proton exchange membrane specific resistance, l is the film thickness, A_{fc} is the active surface area, and λ is the membrane water content.

Finally, considering that the PEMFC system consists of n_{fc} identical cells connected in series, the output voltage of the PEMFC system can be calculated as $V_{stack} = n_{fc}V_{fc}$ and the system output power is $P_{stack} = V_{stack}I_{fc}$.

In the above model, the current I_{fc}, hydrogen pressure P_{H_2}, oxygen pressure P_{O_2}, and temperature T_{fc} are measurable inputs, and the voltage V_{stack} and power P_{stack} are the measurable outputs. I_{max}, l, and A_{fc} are known model parameters. The remaining parameters, including ζ_1, ζ_2, ζ_3, ζ_4, β, R_c, and λ, are unknown and need to be identified.

3. Parameter identification method

3.1. PEMFC model parameter identification problem

The unknown parameters of the semi-empirical PEMFC model presented in Section 2 can be vectorized as

$$x(\zeta_1, \zeta_2, \zeta_3, \zeta_4, \beta, R_c, \lambda) \tag{9}$$

To identify these parameters, we minimize the SSE between the predicted voltage values obtained from the semi-empirical model and the actual voltage values from experimental data. The SSE is easy to calculate, and is often used to evaluate model fitting performance. The more closely SSE approaches zero, the higher the level of fitting precision achieved by the model. In addition, the mean absolute error (MAE) and the root mean square error (RMSE) are used to evaluate the model's overall fitting performance and accuracy. These performance indicators are defined by

$$\mathrm{SSE} = \sum_{j=1}^{M} (V_{\mathrm{r}}^{j} - V_{\mathrm{m}}^{j})^2 \tag{10}$$

$$\mathrm{MAE} = \frac{\sum_{j=1}^{M} \left| V_{\mathrm{r}}^{j} - V_{\mathrm{m}}^{j} \right|}{M} \tag{11}$$

$$\mathrm{RMSE} = \sqrt{\frac{\sum_{j=1}^{M} \left(V_{\mathrm{r}}^{j} - V_{\mathrm{m}}^{j}\right)^2}{M}} \tag{12}$$

where $j \in \{1, 2, \ldots, M\}$ is the index of the data point and M represents the total amount of data points used for model identification. V_{r} and V_{m} are the reference data and model predicted values of the output voltage V_{stack}, respectively. The optimization problem is thus to minimize SSE by tuning the unknown parameters x as defined in (9).

3.2. GWO algorithm

The GWO algorithm is inspired by the group predation of grey wolves in nature. The grey wolf group has a strict hierarchy and unique hunting mechanism, distributed from high to low, in order of α wolf, β wolf, δ wolf, ω wolf, etc. In particular, the α wolf is the core of the wolf pack, which plays a decisive role in the entire wolf pack during hunting, moving, and predating. In nature, the hunting mechanism of the grey wolf group mainly has four parts, including chasing prey, encircling, harassing, and attacking.

When grey wolves hunt, they find and approach prey through the information interaction between individual grey wolves. Considering N wolves in the pack, the position vector of the ith individual wolf in the kth iteration, denoted by x_i^k, is updated by [45]

$$X_n = x_n^k - A_n \cdot \left| C_n \cdot x_n^k - x_i^k \right|, \quad n \in \{\alpha, \beta, \delta\} \tag{13}$$

$$x_i^{k+1} = \frac{X_\alpha + X_\beta + X_\delta}{3} \tag{14}$$

where x_n^k is the position vector of the prey. A_n and C_n are coefficient vectors, given by

$$C_n = 2 \cdot r_1 \tag{15}$$

$$A_n = 2 \cdot a \cdot r_2 - a \tag{16}$$

Here a is the convergence factor that linearly decreases from 2 to 0 with the number of iterations, r_1 and r_2 are random numbers in the range of [0, 1]. After all individual wolves ($i = 1, 2, \ldots, N$) have been updated, the top three best positions with smallest fitness values will be identified and used to update x_α, x_β, x_δ, respectively.

3.3. IGWO algorithm

As seen from the equations presented in Section 3.2, the most striking difference of GWO to the commonly used GA and PSO algorithms lies in the individual position update mode. Using the position information of three optimal individuals (α, β, δ) can effectively avoid the problem of a single local optimal individual during the update of the position of other individuals in the population, thereby enhancing algorithm's global search ability. Although the GWO algorithm is widely recognized as a state-of-the-art metaheuristic optimization technique [35,38], its performance still can be limited by poor population diversity and a tendency to converge to local optima. In the subsequent sections, we will demonstrate that directly applying the conventional GWO algorithm to the PEMFC parameter identification yields low model accuracy.

To address these challenges, we introduce the IGWO algorithm, which incorporates several enhancements. First, chaotic mapping is employed to initialize the population distribution, thereby promoting population diversity. Second, an improved iteration factor based on the cosine function is adopted to balance the global search abilities throughout the early and late stages of the optimization process. Last, in the late iterations, the optimal individual wolf undergoes randomly walking to enhance local search capabilities. As described in the forthcoming sections, the IGWO algorithm offers a simple structure and high implementability, and serves as a proposed solution for effectively addressing the parameter identification problem in the semi-empirical PEMFC model.

The procedure of optimizing the semi-empirical PEMFC model by using the proposed IGWO algorithm is illustrated in Fig. 1, which includes six steps denoted as 'Start', 'Step 1' to 'Step 4', and 'End'. Similar to the traditional GWO algorithm, the 'Start' step configures the hyperparameters, including the total number of iterations (K), population size (N), dimension of the unknown model parameter vector (dim), and range of each model parameter. For the present semi-empirical PEMFC model optimization problem, the dim is set to 7. K and N are set to 800 and 200, respectively, which are tuned according to the actual optimization results. Step 1 serves as the initialization of the population distribution through chaotic mapping. According to the hyperparameters set at the 'Start' step, the chaotic mapping method uniformly distributes grey wolf individuals within the allowable range of model parameters. Step 2 aims to search for the optimal position of the individual and update or retain the optimal position of individual grey wolves (α, β, and δ) by calculating the fitness value of each individual grey wolf in the population. Step 3 implements the elite individual random walk strategy. An improved iterative factor is used to balance the grey wolf population's global and local search capabilities in the early and late stages of the iterative GWO algorithm. The elite individual random walk equation is added in the late stage of the algorithm to enhance the local search capability in the late stage and improve the accuracy of the optimal solution. In Step 4, the individual position update of grey wolves is calculated. Before entering a new iteration, the optimal solution (α wolf position) is extracted at the 'End' step. It should be noted that, 'Step 1' to 'Step 4' in Fig. 1 are the core steps for optimizing the semi-empirical PEMFC model, and the algorithm will be explained in detail next.

Step 1: Chaotic mapping population initialization distribution

The chaotic system possesses inherent characteristics of ergodicity and randomness, which is conducive to improving population diversity and expanding the search space. Therefore, we employ an individual update method based on chaotic logistic variation to initialize the grey wolf individuals. The approach to calculating the position distribution is as follows

$$Z_1 = \mathrm{rand}(1, dim) \tag{17}$$

$$Z_i = c Z_{i-1}(1 - Z_{i-1}) \tag{18}$$

$$x_i^1 = X_{\min} + Z_i(X_{\max} - X_{\min}) \tag{19}$$

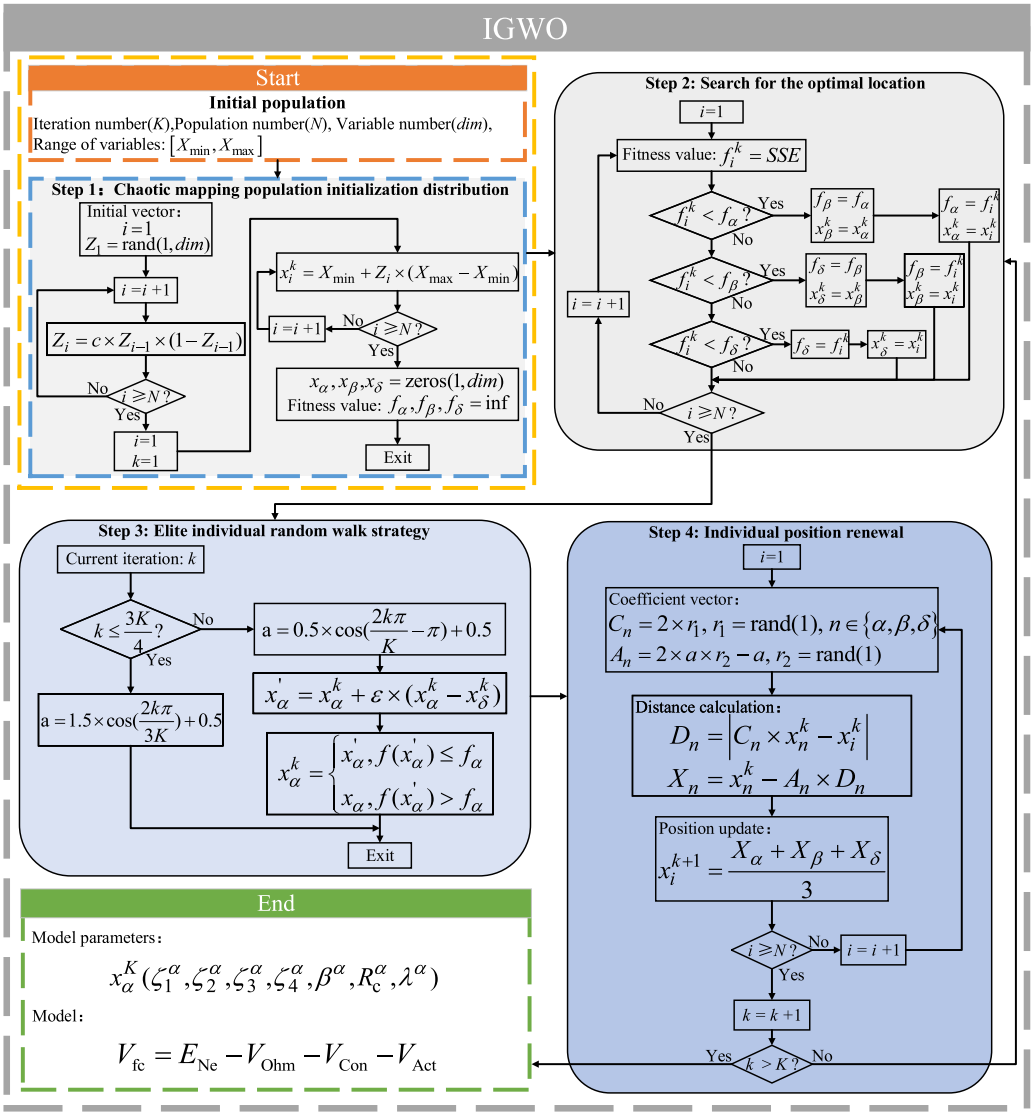

Fig. 1. Flowchart of the proposed IGWO algorithm for PEMFC model parameter identification.

where $c \in [0,4]$ is the chaotic coefficient, $i \in \{1,2,\ldots,N\}$ is the index of individual grey wolf, and Z_i is the vector the chaotic system generates, $Z \in [0,1]$. $X_{\max}$ and $X_{\min}$ are the upper and lower threshold vectors for the parameter vector, respectively. x_i^1 represents the initial position of individual i after chaotic mutation generated at the first iteration.

Step 2: Search for the optimal location

In the first iteration, the three individuals with the best fitness value in the population are selected as grey wolves α, β, and δ, respectively. It can be expressed by

$$f_\alpha(x_\alpha) < f_\beta(x_\beta) < f_\delta(x_\delta) \tag{20}$$

where f_α, f_β, and f_δ present the corresponding fitness values. As the iteration progresses, the position of each individual, denoted by x_i^k, is updated after the calculation of the position in Step 4. The positions of grey wolves α, β, and δ are updated by comparing the optimal fitness values f_α, f_β, and f_δ calculated in the previous iteration.

Step 3: Elite individual random walk strategy

The traditional GWO algorithm's iterative factor decreases linearly, leading to a wide search range for the wolves in the early stage but the range becomes overly narrow in the late stage [40,46]. To address this limitation, a piecewise nonlinear decline function is proposed and designed as follows

$$a = \begin{cases} 1.5\cos\left(\frac{2k\pi}{3K}\right) + 0.5, k \le \frac{3K}{4} \\ 0.5\cos\left(\frac{2k\pi}{K} - \pi\right) + 0.5, k > \frac{3K}{4} \end{cases} \tag{21}$$

where a, k, and K are the iterative convergence factor, the index of the iteration, and the total number of iterations, respectively. The piecewise nonlinear decline function provides a more comprehensive global search range during the early iteration period and a more accurate search range during the late iteration period. To enhance the local search ability of wolves in the late iteration period, we incorporate a random walk strategy for elite individuals to allow for exploration of the search space and improve the chances of finding better solutions locally. This is given by

$$x'_\alpha = x_\alpha^k + \varepsilon(x_\alpha^k - x_\delta^k) \tag{22}$$

where x_α^k and x_δ^k represent the positions of wolves α and δ in the grey wolf population, respectively. ε is the random coefficient uniformly distributed in [0,1]. x'_α denotes the position of wolf α after applying the random walk strategy. The elite individuals of grey wolves search for the best position in a small area. Additionally, the greedy mechanism is employed to compare the position and fitness of elite individuals after migration with the current iteration's optimal position. The new position and fitness value are retained using the following calculation [47]

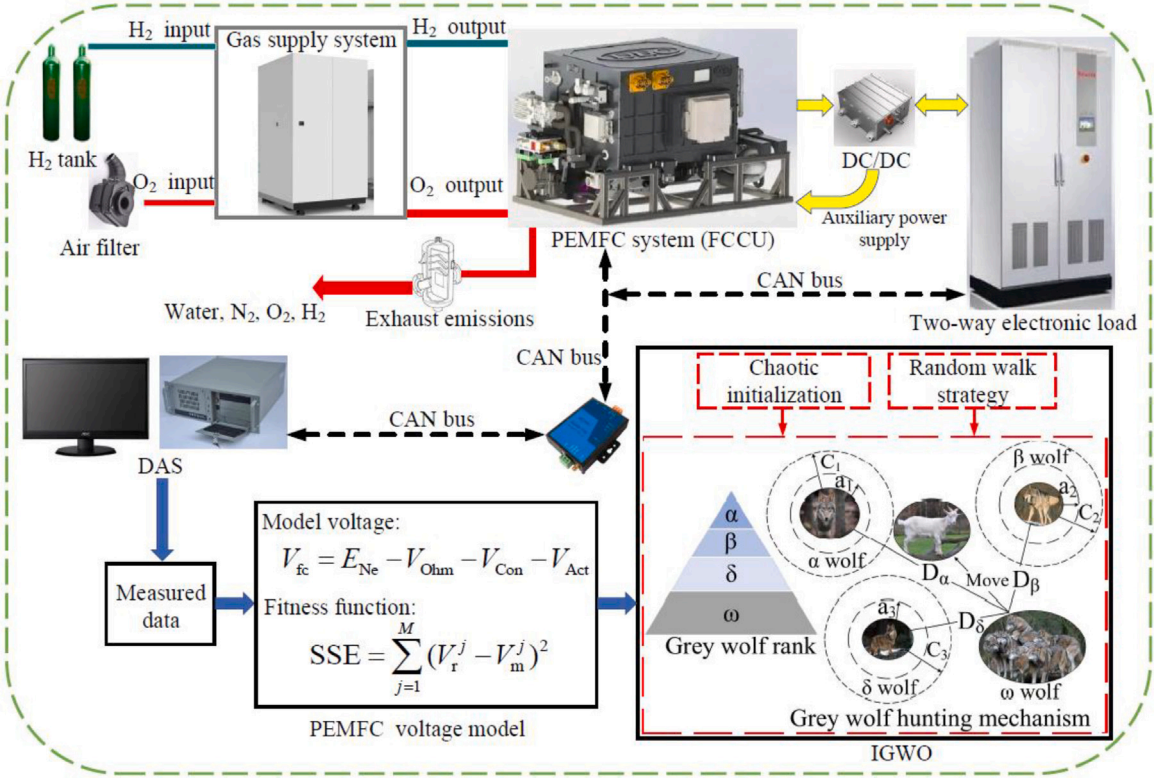

Fig. 2. Framework of the proposed semi-empirical PEMFC model optimized by the IGWO algorithm.

$$x_\alpha^k = \begin{cases} x'_\alpha, f(x'_\alpha) \le f_\alpha \\ x_\alpha^k, f(x'_\alpha) > f_\alpha \end{cases} \tag{23}$$

Step 4: Individual position renewal

Grey wolves search for prey through information interaction between individuals and update their positions according to the position vectors of grey wolves α, β, and δ (denoted by x_α^k, x_β^k, and x_δ^k) when moving. The calculation is the same as in the GWO, i.e.,

$$x_i^{k+1} = \frac{X_\alpha + X_\beta + X_\delta}{3} \tag{24}$$

where

$$X_n = x_n^k - A_n \cdot \left| C_n \cdot x_n^k - x_i^k \right|, \quad n \in \{\alpha, \beta, \delta\} \tag{25}$$

Here, x_i^k and x_i^{k+1} are the position information of individual i at the iterations k and $k+1$, respectively. X_n is the relative position vectors of individual i, and A_n and C_n are corresponding random coefficient vectors as explained in Section 3.2.

4. Experimental verification and analysis

This section begins by analyzing three operating conditions of the 110-kW commercial PEMFC system. Next, the results of model parameter identification using four meta-heuristic methods are discussed. Finally, the model errors under three operating conditions are analyzed.

4.1. PEMFC experiment and conditions

We investigate a 110-kW commercial PEMFC system, and its specifications are given in Table 1. The normal operating temperature of this PEMFC is between 50 °C and 80 °C, the control range of anode hydrogen pressure is from 120 kPa to 270 kPa, and the control range of cathode oxygen pressure is from 110 kPa to 270 kPa. To obtain the operation data of this PEMFC under dynamic operating conditions and establish a semi-empirical PEMFC model, the PEMFC experimental platform and model establishment process is shown in Fig. 2.

Table 1
PEMFC specifications.

PEMFC parameters	Value
Rated power (kW)	110
Operating temperature (°C)	50–80
Hydrogen pressure (kPa)	120–270
Oxygen pressure (kPa)	110–270

The available data include the measurable model inputs and outputs as described in Section 2, i.e., the voltage, current, pressures, and temperature. The fuel cell control unit (FCCU) collects measured data and sends the information to different components via the controller area network (CAN) bus. At the same time, the FCCU communicates with the DC converter to receive the stack voltage and current through the CAN. The data acquisition system (DAS) receives operational data of the PEMFC system transmitted from the FCCU via the CAN bus and stores the data in the computer. The sampling frequency used by the sensor is 1 Hz. The stored current, temperature, and reaction gas pressure are inputs to the semi-empirical PEMFC model established in Section 2, and the output is expressed as the model voltage. The SSE between the model voltage and the actual voltage is used as the fitness function, and the IGWO algorithm minimizes the SSE value to optimize the model parameters.

We use three experimental conditions, denoted by Conditions 1 to 3, to establish and verify the proposed semi-empirical model of the PEMFC system. Condition 1 involves a hybrid experiment lasting 1.39 h, which includes short-term durability and polarization tests. Condition 2 comprises a dynamic durability experiment spanning 4.8 h. Condition 3 is a 2.5 h polarization experiment carried out in accordance with GB/T 24554–2009, which is a Chinese national standard for fuel cell system performance tests [48]. According to GB/T 24554–2009, a minimum of ten power points are uniformly selected within the

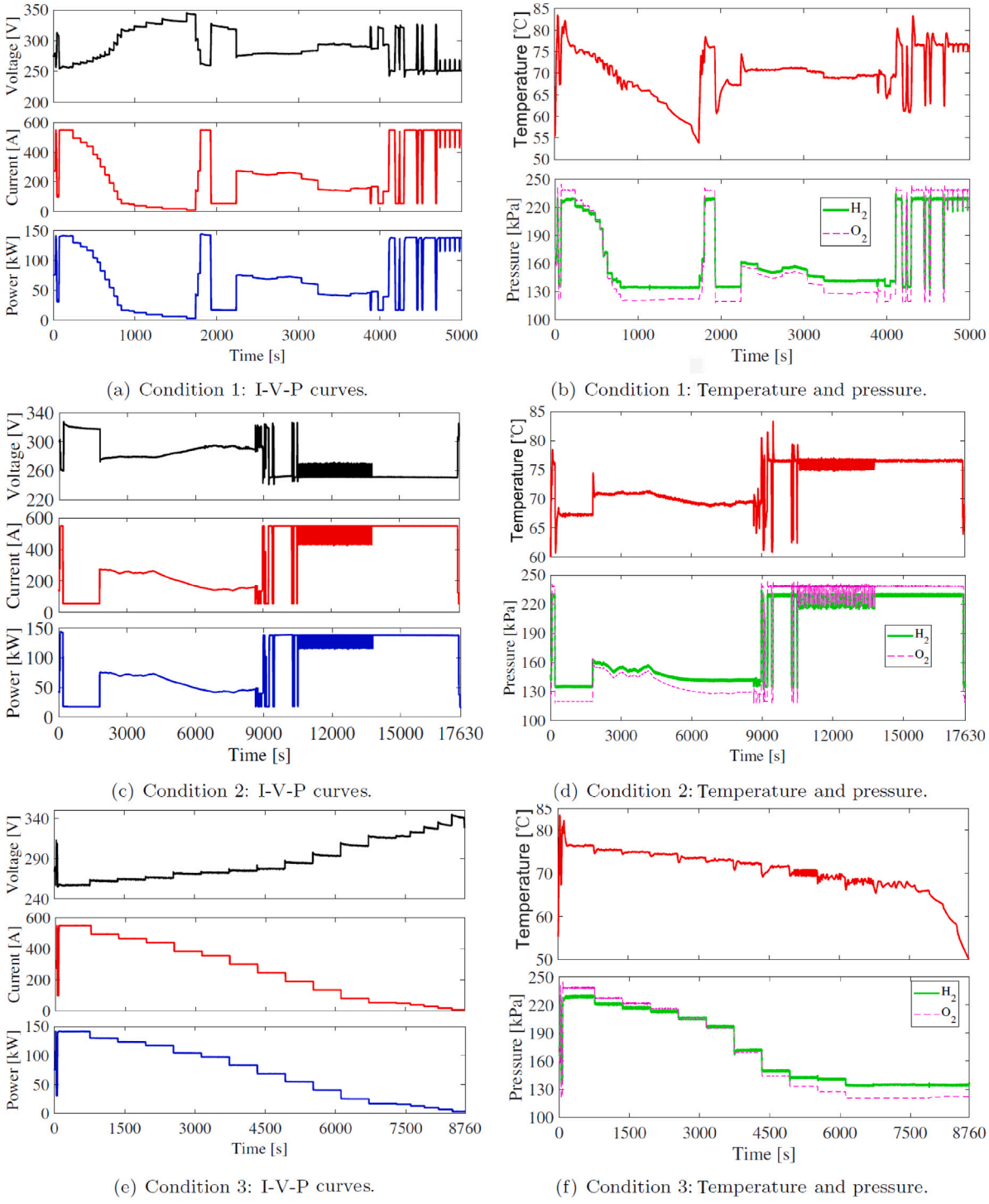

Fig. 3. Measured data of three conditions.

operating range of the fuel cell system. Stable and continuous operation is maintained for at least 3 minutes at each operating point. Therefore, Condition 3 consists of a total of 17 power points.

The ranges and average values of different operating parameters of the PEMFC system under the three conditions are shown in Table 2. These parameters include operating power P_{stack}, voltage V_r, current I_{fc}, hydrogen pressure P_{H_2}, oxygen pressure P_{O_2}, and temperature T_{fc}. The parameter ranges are similar in all three experiments. The power P_{stack} varies between 3.32 kW and 144.53 kW, the voltage V_r ranges from 240.82 V to 345.30 V, the current I_{fc} varies from 9.71 A to 549.84 A, the PEMFC temperature T_{fc} fluctuates between 46.35 °C and 83.50 °C, the hydrogen pressure P_{H_2} changes from 132.12 kPa to 234.28 kPa, and the oxygen pressure P_{O_2} spans from 117.78 kPa to 244.92 kPa. The average values for those parameters, however, show noticeable differences among the three conditions.

The voltage, current, power, temperature, intake hydrogen pressure, and intake oxygen pressure for the three conditions are shown in Fig. 3. It can be seen that the variations of the intake pressure of hydrogen and oxygen over time exhibits similar trends to that of current and power. For instance, in Condition 1 (refer to Fig. 3(a) and (b)), the power, current, voltage, hydrogen pressure, and oxygen pressure all reach their maximum values at approximately 1800 s. Condition 1

Table 2
Condition characteristic parameters.

Condition	Data	P_{stack} (kW)	V_r (V)	I_{fc} (A)	P_{H_2} (kPa)	P_{O_2} (kPa)	T_{fc} (°C)
Condition 1	Max	144.53	345.30	549.82	234.28	244.92	83.50
	Min	3.32	241.06	9.71	132.12	117.78	53.84
	Average	65.91	289.11	244.71	166.05	160.05	70.04
Condition 2	Max	144.53	327.64	549.72	234.28	244.32	83.32
	Min	15.11	240.82	49.22	133.28	117.78	58.77
	Average	91.31	273.17	350.52	185.28	183.76	72.81
Condition 3	Max	141.92	345.30	549.84	230.64	244.92	83.50
	Min	3.32	254.43	9.71	132.12	120.46	46.35
	Average	71.71	286.94	264.59	172.68	167.90	70.58

Table 3
Parameters range of the PEMFC model.

Parameter	ζ_1	ζ_2	ζ_3	ζ_4	β	R_c	λ
Upper limit	−0.5	1×10^{-2}	1×10^{-3}	-1×10^{-5}	1	8×10^{-4}	23
Lower limit	−2	1×10^{-3}	5×10^{-6}	-3×10^{-4}	5×10^{-4}	1×10^{-4}	13

stands out for its wide power operating range, comprehensive data coverage, and high data quality. Therefore, when training the model, utilizing the operating data from Condition 1 enables better model fitting, thereby allowing a semi-empirical model applicable to multiple operating points of PEMFC. It showcases the selected semi-empirical model's fitting capability and enhances its universality. Consequently, Condition 1 is chosen as the parameter identification condition for the model, facilitating a comprehensive description of the model's applicability across a wide range of operating power points.

4.2. Parameter identification result

The parameter identification process is conducted using the experimental data for Condition 1. First, the ranges for the unknown parameters of the semi-empirical PEMFC model are set according to Table 3 [28]. Subsequently, four intelligent algorithms, IGWO, GWO, PSO, and GA, are employed to optimize the semi-empirical PEMFC model. The intelligent optimization is repeatedly performed 20 times.

Fig. 4 displays the SSE of each optimization process. A double-axis plot is utilized to better compare the SSE among the four parameter identification methods. When comparing IGWO, GWO, PSO, and GA, it is evident that GA exhibits large and unstable SSE values, indicating low optimization accuracy. The SSE values optimized by PSO are similar to GWO, but the SSE still exhibit instability. The SSE value range is divided into $[0.28, 0.29)$, $[0.29, 0.3)$, $[0.3, 0.31)$, and $[0.31, +\infty)$. Within the range of $[0.28, 0.29)$, the IGWO algorithm accounts for 70%, while the GWO represents 30%, and the PSO and the GA are both zero. Compared to the GWO algorithm, PSO and GA demonstrate significantly weaker optimization abilities. The IGWO algorithm effectively enhances the accuracy and stability of the GWO algorithm, as evidenced by the SSE value and probability distribution.

For model verification, the model parameters corresponding to the minimum SSE values of the four algorithms are selected and presented in Table 4, along with the computational time of each model. Under Condition 1, the running time of the four algorithms is similar, with the IGWO algorithm not significantly increasing the computational time compared to the traditional GWO algorithm. While the convergence time of the IGWO is slightly longer than that of the GWO, it is still shorter than that of the PSO and GA. In the subsequent analysis, we will utilize these optimized model parameters to evaluate the accuracy and versatility of the four PEMFC models.

4.3. Model error analysis

In this subsection, Conditions 1 to 3 are used to assess the accuracy, versatility, and generalization of the proposed models. With a slight

Table 4
PEMFC model parameters optimized with four identification methods.

Parameter	ζ_1	ζ_2	ζ_3	ζ_4	β	R_c	λ	Runtime
Unit	–	$\times 10^{-3}$	$\times 10^{-4}$	$\times 10^{-4}$	$\times 10^{-4}$	$\times 10^{-4}$	–	s
IGWO	−1.29	7.66	3.30	−1.15	5.88	2.85	22.95	948.4
GWO	−1.31	8.45	3.83	−1.11	20.04	3.10	22.59	947.9
PSO	−1.34	6.70	2.44	−1.37	10.00	1.32	13.00	954.2
GA	−1.93	9.28	3.13	−0.99	19.77	3.41	19.18	962.3

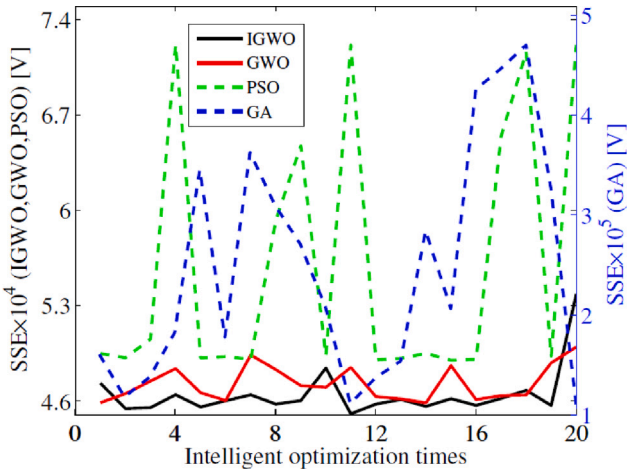

Fig. 4. Optimizing SSE value for 20 times.

abuse of terminology, in the following context, we denote a model whose parameters are optimized by IGWO, GWO, PSO, and GA as the IGWO model, GWO model, PSO model, and GA model, respectively.

Figs. 5(a), 6(a), and 7(a) illustrate the output voltage of PEMFC models based on four parameter identification methods under Conditions 1 to 3, while Figs. 5(b), 6(b), and 7(b) present the corresponding model errors. The overlapping areas of the results for the four models have been partially enlarged to enhance clarity. It can be observed that all models effectively capture the voltage change trend.

Specifically, Condition 1 serves as the foundation for establishing the model. The resultant output voltage and model error are displayed in Fig. 5. As observed from Fig. 5(a), the GA model demonstrates low accuracy, while IGWO, GWO, and PSO models closely replicate the original voltage curve. Model errors are shown in Fig. 5(b). Voltage errors of IGWO, GWO, and PSO models predominantly fall between −5 V and 5 V, while the voltage errors of GA models span from −5 V to 10 V. The maximum voltage error (MAX), MAE, and RMSE of the

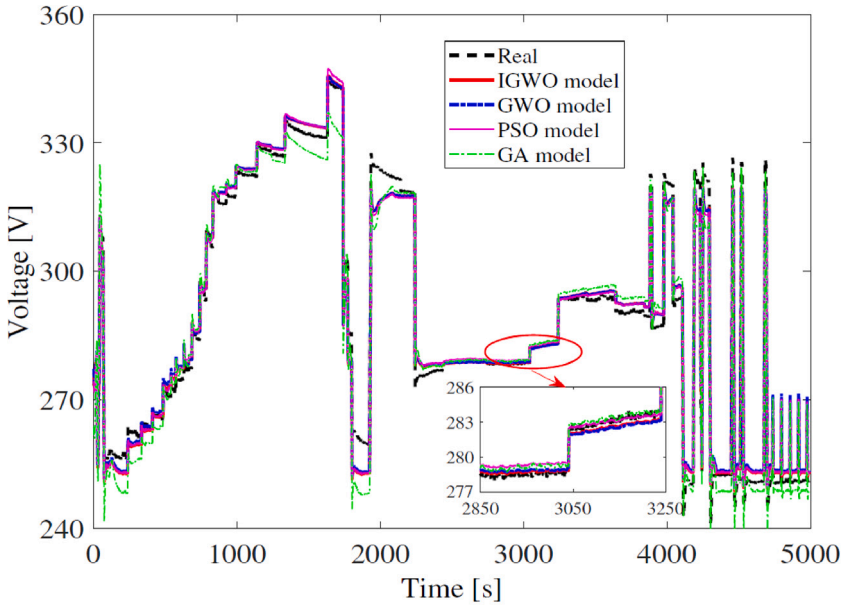

(a) Voltage.

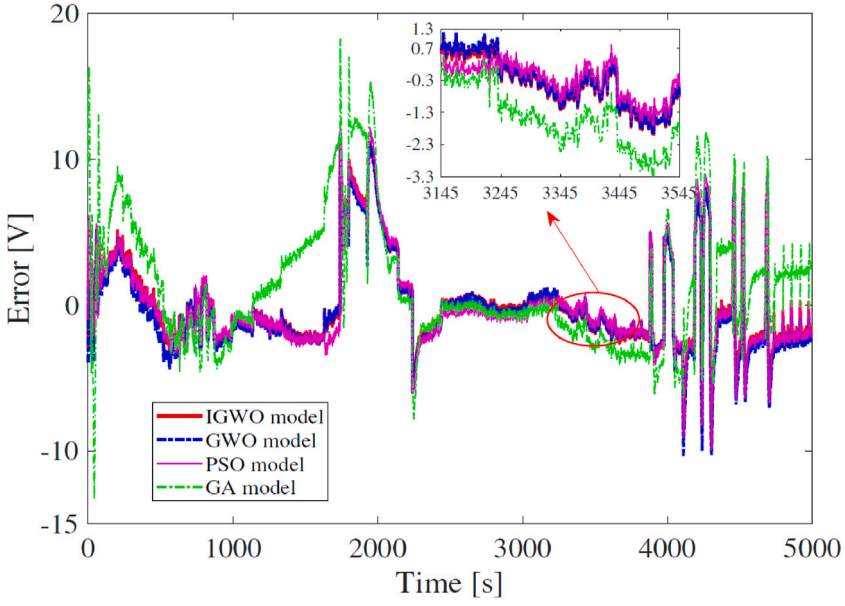

(b) Model error.

Fig. 5. Comparison of four models under Condition 1.

four models are compared in Table 5. The MAX of the IGWO, GWO, and PSO models are 11.59 V, 11.87 V, and 12.37 V, respectively, significantly lower than that of the GA model. The MAE and RMSE of the IGWO model are 2.17 V and 3.01 V, respectively, smaller than the other three models. The MAE and RMSE of the GWO model are 2.25 V and 3.05 V, respectively, smaller than the PSO model. Therefore, the IGWO model outperforms in terms of minimal overall error and high numerical stability, rendering it better suited for accurately capturing the actual PEMFC output performance.

Conditions 2 and 3 are utilized for model verification. The predicted voltage and model error are shown in Figs. 6 and 7, respectively. Similarly to the findings in Condition 1, Fig. 6(a) and Fig. 7(a) reveals the limited accuracy of the GA model, whereas IGWO, GWO, and PSO models closely align with the original voltage curve. Model errors corresponding to Conditions 2 and 3 are shown in Fig. 6(b) and Fig. 7(b), respectively. All four models demonstrate substantial errors when subjected to extremely high and low load currents. As shown in Table 5, the GA model exhibits a considerably higher MAX of 18.26 V and 16.36 V under Conditions 2 and 3, respectively, exceeding those of the other three models. In Condition 2, the MAE and RMSE of the IGWO model are 1.57 V and 2.12 V, respectively, which are the lowest amongst all models. The MAE and RMSE of the GWO model are 1.82 V and 2.35 V, respectively, smaller than the PSO model. In Condition 3, the MAE and RMSE of the IGWO model are 1.91 V and 2.15 V, respectively, lower than those of the GWO model but slightly higher than that of the PSO model. In addition, the MAX of the IGWO model is 5.42 V, smaller than the PSO model's 6.15 V. These results emphasize the fluctuation of model error influenced by the specific operating conditions. Nevertheless, the outcomes indicate that IGWO effectively optimizes the semi-empirical PEMFC model under both Conditions 2 and 3 during the verification process. The fitting accuracy of the IGWO model is higher than that of the GWO model across all three operating conditions. Moreover, in comparison to the PSO and GA models, the

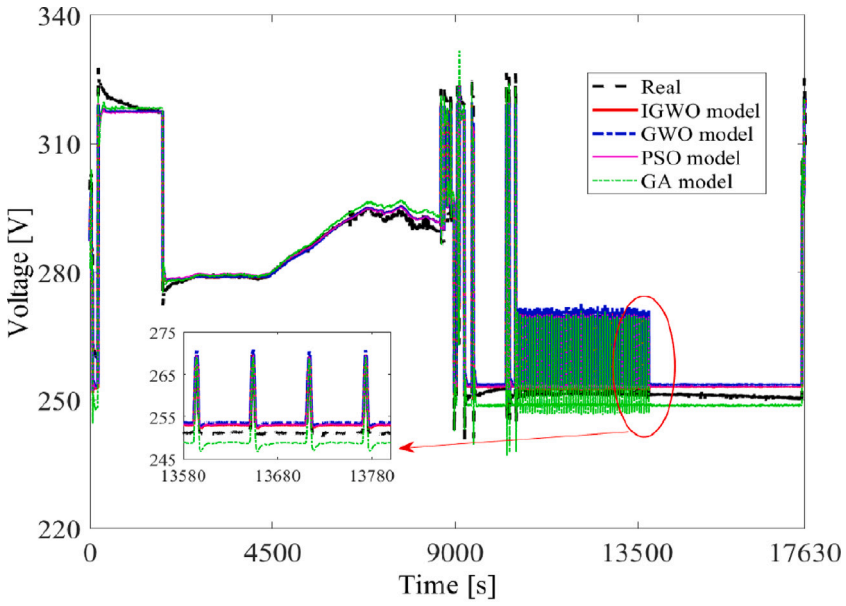

(a) Voltage.

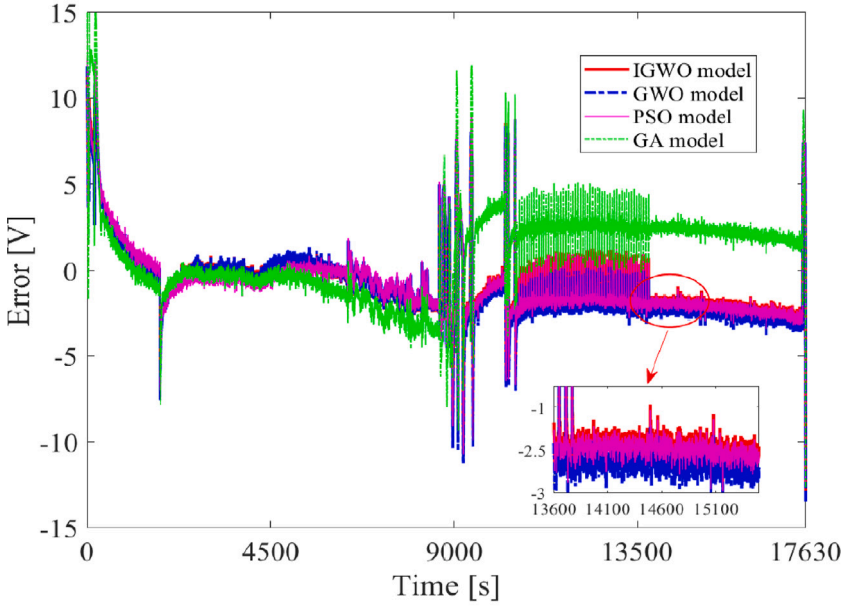

(b) Model error.

Fig. 6. Comparison of four models under Condition 2.

IGWO model features a simpler structure with fewer parameters to be configured.

5. Conclusion

This paper presents an IGWO algorithm for identifying parameters in a proposed semi-empirical PEMFC model. This approach addresses the limitations inherent in the traditional GWO algorithm. Furthermore, to evaluate the effectiveness and practicability of the IGWO algorithm, the experimental data obtained from a 110-kW commercial PEMFC system under highly dynamic operating conditions were divided into several parts for model establishment and verification. The primary research findings are summarized below:

(1) When initializing the population distribution, the IGWO algorithm uses chaotic mapping to optimize the traditional GWO algorithm.

Table 5
Error analysis of four models under three conditions.

Condition	Model	MAX	MAE	RMSE
Condition 1	IGWO	11.59	2.17	3.01
	GWO	11.87	2.25	3.05
	PSO	12.37	2.27	3.14
	GA	18.26	3.16	4.45
Condition 2	IGWO	13.30	1.57	2.12
	GWO	13.50	1.82	2.35
	PSO	12.58	1.68	2.23
	GA	18.26	2.09	2.76
Condition 3	IGWO	5.42	1.91	2.15
	GWO	5.21	2.01	2.29
	PSO	6.15	1.87	2.11
	GA	16.36	3.44	4.31

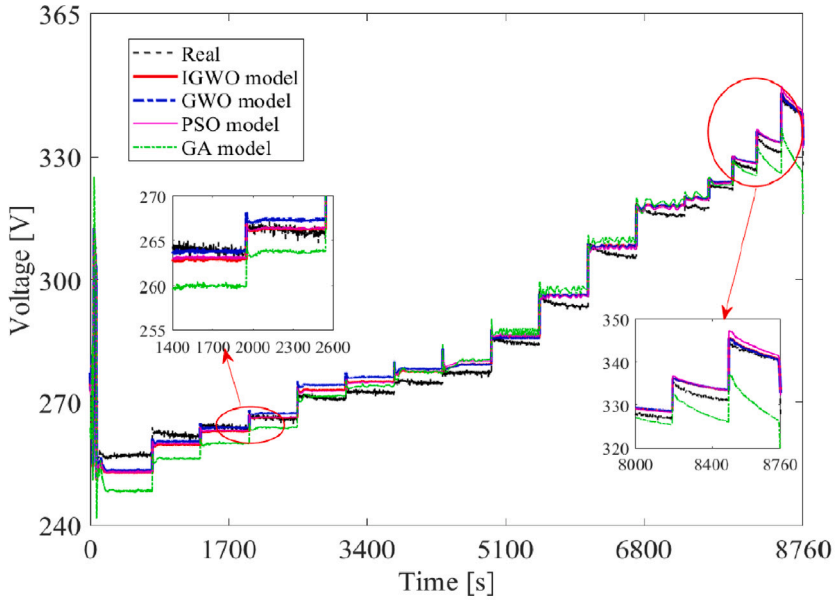

(a) Voltage.

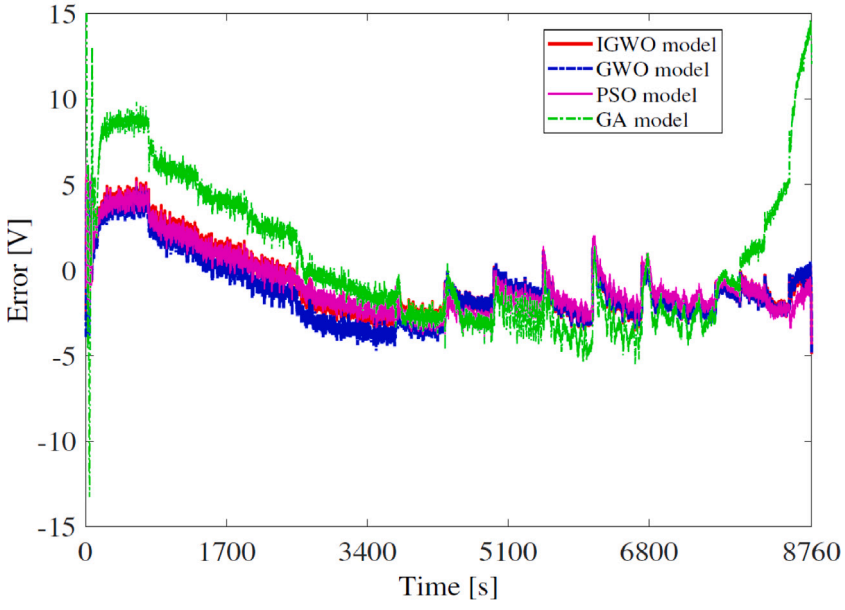

(b) Model error.

Fig. 7. Comparison of four models under Condition 3.

Compared to initializing the distribution using random numbers, chaotic mapping can evenly distribute the population position and improve the diversity and convergence speed of the population.

(2) An adaptive iterative factor, improved through the utilization of the cosine function, was designed to balance the search capabilities of the grey wolf population during both initial and later stages. Additionally, a random walk strategy was introduced for elite individuals of the grey wolf in the later iterations of the algorithm, thereby enhancing the local search capabilities.

(3) An analysis was given focused on the fitting accuracy of the semi-empirical model optimized by IGWO, GWO, PSO, and GA algorithms. Simulation results show that, under verification conditions, the IGWO algorithm can retain the MAX, MAE, and RMSE of the predicted PEMFC voltage within 13.30 V, 2.17 V, and 3.01 V, respectively.

Compared to state-of-the-art GWO, PSO, and GA, the IGWO algorithm offers the merits of simpler structure, minimum efforts for hyperparameter setting, easy implementation, and high predictive accuracy. These attributes highlight that IGWO is well-suited for semi-empirical PEMFC model optimization at dynamic operation. The demonstrated advantages of the IGWO algorithm also suggest its applicability extends to various engineering challenges, including solving the problems of path optimization and energy allocation.

This paper also reveals that a single semi-empirical model cannot sufficiently capture all the PEMFC output characteristics. Establishing a generic model capable of accommodating more dynamic operations is the basis of more comprehensive PEMFC modeling and advanced control. Therefore, forthcoming research on the PEMFC model should be focused on two principal aspects: identifying and prioritizing the

influence of different factors on the output characteristics and establishing a versatile control-oriented model tailored for the PEMFC system.

CRediT authorship contribution statement

Hongxu Zhou: Writing – original draft, Software, Data curation. **Xiaohua Wu:** Methodology, Funding acquisition, Conceptualization. **Yang Li:** Writing – review & editing. **Zhanfeng Fan:** Writing – original draft, Project administration, Methodology. **Weishan Chen:** Resources, Data curation. **Jianwei Mao:** Software, Formal analysis. **Pengyi Deng:** Supervision, Methodology. **Torsten Wik:** Writing – review & editing.

Declaration of competing interest

The authors declare that they have no known competing financial interests or personal relationships that could have appeared to influence the work reported in this paper.

Data availability

Data will be made available on request.

Acknowledgments

This work was supported in part by Science and Technology Department of Sichuan Province (Grant Nos. 2023YFG0067, 2023YFG0068), Xihua University Fund (Grant No. QCCK2022-001), China Scholarship Council (CSC No. 202105530027).

References

[1] Di Micco S, Mastropasqua L, Cigolotti V, Minutillo M, Brouwer J. A framework for the replacement analysis of a hydrogen-based polymer electrolyte membrane fuel cell technology on board ships: A step towards decarbonization in the maritime sector. Energy Convers Manage 2022;267:115893. http://dx.doi.org/10.1016/j.enconman.2022.115893.

[2] Correa G, Munoz PM, Rodriguez CR. A comparative energy and environmental analysis of a diesel, hybrid, hydrogen and electric urban bus. Energy 2019;187:115906. http://dx.doi.org/10.1016/j.energy.2019.115906.

[3] Wang G, Yu Y, Liu H, Gong C, Wen S, Wang X, Tu Z. Progress on design and development of polymer electrolyte membrane fuel cell systems for vehicle applications: a review. Fuel Process Technol 2018;179:203–28. http://dx.doi.org/10.1016/j.fuproc.2018.06.013.

[4] Mitra U, Arya A, Gupta S. A comprehensive and comparative review on parameter estimation methods for modelling proton exchange membrane fuel cell. Fuel 2023;335:127080. http://dx.doi.org/10.1016/j.fuel.2022.127080.

[5] Zhou H, Yu Z, Wu X, Fan Z, Yin X, Zhou L. Dynamic programming improved online fuzzy power distribution in a demonstration fuel cell hybrid bus. Energy 2023;284:128549. http://dx.doi.org/10.1016/j.energy.2023.128549.

[6] Deng Z, Chen Q, Zhang L, Zong Y, Zhou K, Fu Z. Control oriented data driven linear parameter varying model for proton exchange membrane fuel cell systems. Appl Energy 2020;277:115540. http://dx.doi.org/10.1016/j.apenergy.2020.115540.

[7] Li H, Qiao B, Liu J, Yang Y, Fan W, Lu G. A data-driven framework for performance prediction and parameter optimization of a proton exchange membrane fuel cell. Energy Convers Manage 2022;271:116338. http://dx.doi.org/10.1016/j.enconman.2022.116338.

[8] Ohenoja M, Leiviska K. Observations on the parameter estimation problem of polymer electrolyte membrane fuel cell polarization curves. Fuel Cells 2020;20(5):516–26. http://dx.doi.org/10.1002/fuce.201900155.

[9] Sultan HM, Menesy AS, Hassan M, Jurado F, Kamel S. Standard and quasi oppositional bonobo optimizers for parameter extraction of PEM fuel cell stacks. Fuel 2023;340:127586. http://dx.doi.org/10.1016/j.fuel.2023.127586.

[10] Abd Elaziz M, Abualigah L, Issa M, Abd El-Latif AA. Optimal parameters extracting of fuel cell based on Gorilla Troops Optimizer. Fuel 2023;332:126162. http://dx.doi.org/10.1016/j.fuel.2022.126162.

[11] Han I, Chung C. A hybrid model combining a support vector machine with an empirical equation for predicting polarization curves of PEM fuel cells. Int J Hydrogen Energy 2017;42(10):7023–8. http://dx.doi.org/10.1016/j.ijhydene.2017.01.131.

[12] Zhu G, Chen W, Lu S, Chen X. Parameter study of high-temperature proton exchange membrane fuel cell using data-driven models. Int J Hydrogen Energy 2019;44(54):28958–67. http://dx.doi.org/10.1016/j.ijhydene.2019.09.115.

[13] Feng S, Huang W, Huang Z, Jian Q. Optimization of maximum power density output for proton exchange membrane fuel cell based on a data-driven surrogate model. Appl Energy 2022;317:119158. http://dx.doi.org/10.1016/j.apenergy.2022.119158.

[14] Pourkiaei SM, Ahmadi MH, Hasheminejad SM. Modeling and experimental verification of a 25W fabricated PEM fuel cell by parametric and GMDH-type neural network. Mech Ind 2016;17(1):105. http://dx.doi.org/10.1051/meca/2015050.

[15] Guo C, Lu J, Tian Z, Guo W, Darvishan A. Optimization of critical parameters of PEM fuel cell using TLBO-DE based on Elman neural network. Energy Convers Manage 2019;183:149–58. http://dx.doi.org/10.1016/j.enconman.2018.12.088.

[16] Qi Y, Andersson M, Wang L, Wang J. System behavior prediction by artificial neural network algorithm of a methanol steam reformer for polymer electrolyte fuel cell stack use. Fuel Cells 2021;21(3):279–89. http://dx.doi.org/10.1002/fuce.202100006.

[17] Cheng Y, Zerhouni N, Lu C. A hybrid remaining useful life prognostic method for proton exchange membrane fuel cell. Int J Hydrogen Energy 2018;43(27):12314–27. http://dx.doi.org/10.1016/j.ijhydene.2018.04.160.

[18] Zhu W, Guo B, Li Y, Yang Y, Xie C, Jin J, Gooi HB. Uncertainty quantification of proton-exchange-membrane fuel cells degradation prediction based on Bayesian-gated recurrent unit. eTransportation 2023;16:100230. http://dx.doi.org/10.1016/j.etran.2023.100230.

[19] Yang Y, Zhu W, Li Y, Zhao B, Zhang L, Song J, Deng Z, Shi Y, Xie C. Modeling of PEMFC and analysis of multiple influencing factors on output characteristics. J Electrochem Soc 2022;169(3):034507. http://dx.doi.org/10.1149/1945-7111/AC580A.

[20] Amphlett JC, Baumert RM, Mann RF, Peppley BA, Roberge PR, Harris TJ. Performance modeling of the ballard mark IV solid polymer electrolyte fuel cell: I . Mechanistic model development. J Electrochem Soc 1995;142(1):1. http://dx.doi.org/10.1149/1.2043866.

[21] Restrepo C, Konjedic T, Garces A, Calvente J, Giral R. Identification of a proton-exchange membrane fuel cell's model parameters by means of an evolution strategy. IEEE Trans Ind Inf 2015;11(2):548–59. http://dx.doi.org/10.1109/TII.2014.2317982.

[22] Han J, Yu S, Yi S. Oxygen excess ratio control for proton exchange membrane fuel cell using model reference adaptive control. Int J Hydrogen Energy 2019;44(33):18425–37. http://dx.doi.org/10.1016/j.ijhydene.2019.05.041.

[23] Wang Z, Mao J, He Z, Liang F. Fuzzy control based on IQPSO in proton-exchange membrane fuel-cell Temperature system. J Energy Eng 2020;146(5):04020044. http://dx.doi.org/10.1061/(ASCE)EY.1943-7897.0000691.

[24] Gong C, Xing L, Liang C, Tu Z. Modeling and dynamic characteristic simulation of air-cooled proton exchange membrane fuel cell stack for unmanned aerial vehicle. Renew Energy 2022;188:1094–104. http://dx.doi.org/10.1016/j.renene.2022.02.104.

[25] Aly M, Rezk H. A differential evolution-based optimized fuzzy logic MPPT method for enhancing the maximum power extraction of proton exchange membrane fuel cells. IEEE Access 2020;8:172219–32. http://dx.doi.org/10.1109/ACCESS.2020.3025222.

[26] Sun Z, Wang N, Bi Y, Srinivasan D. Parameter identification of PEMFC model based on hybrid adaptive differential evolution algorithm. Energy 2015;90:1334–41. http://dx.doi.org/10.1016/j.energy.2015.06.081.

[27] Sun Z, Cao D, Ling Y, Xiang F, Sun Z, Wu F. Proton exchange membrane fuel cell model parameter identification based on dynamic differential evolution with collective guidance factor algorithm. Energy 2021;216:119056. http://dx.doi.org/10.1016/j.energy.2020.119056.

[28] Ohenoja M, Leiviska K. Validation of genetic algorithm results in a fuel cell model. Int J Hydrogen Energy 2010;35(22):12618–25. http://dx.doi.org/10.1016/j.ijhydene.2010.07.129.

[29] Priya K, Sudhakar Babu T, Balasubramanian K, Sathish Kumar K, Rajasekar N. A novel approach for fuel cell parameter estimation using simple genetic algorithm. Sustain Energy Technol Assess 2015;12:46–52. http://dx.doi.org/10.1016/j.seta.2015.09.001.

[30] Salim R, Nabag M, Noura H, Fardoun A. The parameter identification of the Nexa 1.2 kW PEMFC's model using particle swarm optimization. Renew Energy 2015;82:26–34. http://dx.doi.org/10.1016/j.renene.2014.10.012.

[31] Liu E, Hung Y, Hong C. Improved metaheuristic optimization algorithm applied to hydrogen fuel cell and photovoltaic cell parameter extraction. Energies 2021;14(3):619. http://dx.doi.org/10.3390/en14030619.

[32] Ozdemir MT. Optimal parameter estimation of polymer electrolyte membrane fuel cells model with chaos embedded particle swarm optimization. Int J Hydrogen Energy 2021;46(30):16465–80. http://dx.doi.org/10.1016/j.ijhydene.2020.12.203.

[33] Rao Y, Shao Z, Ahangarnejad AH, Gholamalizadeh E, Sobhani B. Shark smell optimizer applied to identify the optimal parameters of the proton exchange membrane fuel cell model. Energy Convers Manage 2019;182:1–8. http://dx.doi.org/10.1016/j.enconman.2018.12.057.

[34] Rezaie M, Azar KK, Sani AK, Akbari E, Ghadimi N, Razmjooy N, Ghadamyari M. Model parameters estimation of the proton exchange membrane fuel cell by a modified golden jackal optimization. Sustain Energy Technol Assess 2022;53(C):102657. http://dx.doi.org/10.1016/j.seta.2022.102657.

[35] Ali M, El-Hameed MA, Farahat MA. Effective parameters' identification for polymer electrolyte membrane fuel cell models using grey wolf optimizer. Renew Energy 2017;111:455–62. http://dx.doi.org/10.1016/j.renene.2017.04.036.
[36] Vamsi Krishna Reddy AK, Venkata Lakshmi Narayana K. Meta-heuristics optimization in electric vehicles -an extensive review. Renew Sustain Energy Rev 2022;160:112285. http://dx.doi.org/10.1016/j.rser.2022.112285.
[37] Tikhamarine Y, Souag-Gamane D, Najah Ahmed A, Kisi O, El-Shafie A. Improving artificial intelligence models accuracy for monthly streamflow forecasting using grey Wolf optimization (GWO) algorithm. J Hydrol 2020;582:124435. http://dx.doi.org/10.1016/j.jhydrol.2019.124435.
[38] Ghalambaz M, Jalilzadeh Yengejeh R, Davami AH. Building energy optimization using grey wolf optimizer (GWO). Case Stud Therm Eng 2021;27:101250. http://dx.doi.org/10.1016/j.csite.2021.101250.
[39] Rawat N, Thakur P, Singh AK, Bhatt A, Sangwan V, Manivannan A. A new grey wolf optimization-based parameter estimation technique of solar photovoltaic. Sustain Energy Technol Assess 2023;57:103240. http://dx.doi.org/10.1016/j.seta.2023.103240.
[40] Miao D, Chen W, Zhao W, Demsas T. Parameter estimation of PEM fuel cells employing the hybrid grey wolf optimization method. Energy 2020;193:571–82. http://dx.doi.org/10.1016/j.energy.2019.116616.
[41] Hao P, Sobhani B. Application of the improved chaotic grey wolf optimization algorithm as a novel and efficient method for parameter estimation of solid oxide fuel cells model. Int J Hydrogen Energy 2021;46(73):36454–65. http://dx.doi.org/10.1016/j.ijhydene.2021.08.174.
[42] Liu J, Wei X, Huang H. An improved grey wolf optimization algorithm and its application in path planning. IEEE Access 2021;9:121944–56. http://dx.doi.org/10.1109/ACCESS.2021.3108973.
[43] Wang G, Gao J. Parallel conjugate gradient-particle swarm optimization and the parameters design based on the polygonal fuzzy neural network. J Intell Fuzzy Systems 2019;37(1):1477–89. http://dx.doi.org/10.3233/JIFS-182882.
[44] Zhenxing Z, Rennong Y, Huanyu L, Yuhuan F, Zhenyu H, Ying Z. Antlion optimizer algorithm based on chaos search and its application. J Syst Eng Electron 2019;30(2):352–65. http://dx.doi.org/10.21629/JSEE.2019.02.14.
[45] Mirjalili S, Mirjalili SM, Lewis A. Grey wolf optimizer. Adv Eng Softw 2014;69:46–61. http://dx.doi.org/10.1016/j.advengsoft.2013.12.007.
[46] Wang E, Xia J, Li J, Sun X, Li H. Parameters exploration of SOFC for dynamic simulation using adaptive chaotic grey wolf optimization algorithm. Energy 2022;261:125146. http://dx.doi.org/10.1016/j.energy.2022.125146.
[47] Adhikary J, Acharyya S. Randomized Balanced Grey Wolf Optimizer (RBGWO) for solving real life optimization problems. Appl Soft Comput 2022;117:108429. http://dx.doi.org/10.1016/j.asoc.2022.108429.
[48] Performance test methods for fuel cell engines. National standard of the people's republic of china, Standardization Administration of the People's Republic of China; 2009, https://www.chinesestandard.net/PDF.aspx/GBT24554-2009.